ELSEVIER

Journal of Organometallic Chemistry 490 (1995) 173–178

Journal of Organometallic Chemistry

Synthesis and characterisation of the methylene-inserted mixed-chalcogenide compounds $Fe_2(CO)_6(\mu\text{-}SeCH_2Te)$ and $Fe_2(CO)_6(\mu\text{-}SCH_2Te)$

Pradeep Mathur [a,*], Bala. Manimaran [a], Md. Munkir Hossain [a], Rupa Shanbag [a], Jayshree Murthy [a], Iyer S. Saranathan [a], C.V.V. Satyanarayana [b], Mohan M. Bhadbhade [c]

[a] *Department of Chemistry, Indian Institute of Technology, Powai, Bombay 400 076, India*
[b] *Regional Sophisticated Instrumentation Centre, Indian Institute of Technology, Powai, Bombay 400 076, India*
[c] *Central Salt and Marine Chemicals Research Institute, Bhavnagar 364 002, India*

Received 1 August 1994

Abstract

The methylene-bridged, mixed-chalcogen compounds $Fe_2(CO)_6(\mu\text{-}SeCH_2Te)$ (**1**) and $Fe_2(CO)_6(\mu\text{-}SCH_2Te)$ (**3**) have been synthesised from the room temperature reaction of diazomethane with $Fe_2(CO)_6(\mu\text{-}SeTe)$ and $Fe_2(CO)_6(\mu\text{-}STe)$, respectively. Compounds **1** and **3** have been characterised by IR, ^1H, ^{13}C, ^{77}Se and ^{125}Te NMR spectroscopy. The structure of **1** has been elucidated by X-ray crystallography. The crystals are monoclinic, space group $P2_1/n$, $a = 6.695(2)$, $b = 13.993(5)$, $c = 14.007(4)$ Å, $\beta = 103.03(2)°$, $V = 1278(7)$ Å^3, $Z = 4$, $D_c = 2.599$ g cm^{-3} and $R = 0.030$ ($R_w = 0.047$).

Keywords: Iron; Tellurium; Selenium; Chalcogenide; X-ray diffraction; Crystal structure

1. Introduction

Single atom, Main Group elements are recognised as important ligands in transition metal chemistry [1]. The chalcogen atoms have been amongst the most useful bridging and stabilising ligands in numerous metal carbonyl compounds [2]. Early work in metal–chalcogenide complexes suggested that while sulphur and selenium show similar behaviour, the reactivity of tellurium is often unique. Recently, however, it has become evident that selenium displays unique reactivity features in its iron compounds towards small organic molecules. For example, acetylene activation on $Fe_2(CO)_6(\mu\text{-}Se_2)$ occurs such that there is a stepwise reduction of the acetylenic triple bond to a single bond [3]. Such a stepwise process was not observed when $Fe_2(CO)_6(\mu\text{-}S_2)$ or $Fe_2(CO)_6(\mu\text{-}Te_2)$ were used. Moreover, the unusual mixed-metal compound $(CO)_6Fe_2Pt(PPh_3)_2\{\mu\text{-}SeC(Ph)C(H)Se\}$ has been isolated and characterised structurally [4]; the S and Te analogues of this are not known. In previous reports we have described the reaction of diazomethane with $Fe_2(CO)_6(\mu\text{-}Te_2)$ [5] and $Fe_3(CO)_9(\mu_3\text{-}Te)_2$ [6]. Here, we report on the insertion of methylene groups into the Se–Te and S–Te bonds of $Fe_2(CO)_6(\mu\text{-}SeTe)$ and $Fe_2(CO)_6(\mu\text{-}STe)$, respectively.

2. Results and discussion

The mixed-chalcogen compounds, $Fe_2(CO)_6(\mu\text{-}EE')$ [E = S, Se; E' = Te] were prepared by the reaction of basic methanolic solution of $Fe(CO)_5$ with an aqueous solution of a mixture of Na_2EO_3 and $Na_2E'O_3$, followed by acidification, treatment with NaOMe and chromatographic work-up [7,8].

2.1. Reaction of $Fe_2(CO)_6(\mu\text{-}SeTe)$ with diazomethane

The reaction of $Fe_2(CO)_6(\mu\text{-}SeTe)$ with diazomethane was carried out using a method [9] which involved distilling an ethereal solution of diazomethane directly into the ethereal solution of $Fe_2(CO)_6(\mu\text{-}SeTe)$

* Corresponding author.

SSDI 0022-328X(94)05165-8

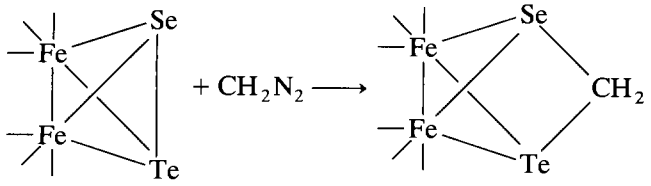

Scheme 1. Formation of compound **1**.

(Scheme 1). The reaction was monitored by TLC and IR spectroscopy. As soon as the disappearance of the reactant was observed, the addition of diazomethane was stopped. Chromatographic work-up on silica gel TLC plates yielded five bands. Of these, the third and fourth bands were major bands and were isolated. The other bands could not be obtained in sufficient amounts for characterisation.

On the basis of IR, NMR (Table 1) and elemental analysis, the third band has been identified as $Fe_2(CO)_6(\mu\text{-}SeCH_2Te)$ (**1**). The fourth band was identified as the previously reported $Fe_2(CO)_6(\mu\text{-}TeCH_2Te)$ (**2**), based on its infrared spectrum in the carbonyl region [5]. Compound **1** displayed an infrared spectrum in the carbonyl region which was similar to that of **2**, with a shift of the frequencies to higher values. The ^1H NMR spectrum of **1** showed a single peak for the CH_2 protons at δ 3.13 ppm with ^{125}Te satellites ($^2J_{H-Te} = 25$ Hz). In **2** and $Fe_2(CO)_6(\mu\text{-}SeCH_2Se)$ (**4**) [10], the CH_2 signals were seen at δ 2.19 and δ 4.02 ppm, respectively. The ^1H-coupled ^{13}C NMR spectrum of **1** showed a triplet centred at δ −16.6 ppm ($^1J_{C-H} = 159$ Hz) for the CH_2 group and a single peak at δ 210.4 ppm due to the CO groups. The ^{13}C NMR spectra of **2** and **4** showed signals for the CH_2 groups at δ −64.9 and δ 27.5 ppm, respectively. The ^{77}Se NMR spectrum of **1** showed a signal at δ 189.7 ppm (t, $^2J_{Se-H} = 10$ Hz), as expected, downfield of the signal seen at δ 67.6 ppm (t, $^2J_{Se-H} = 10$ Hz) in the ^{77}Se NMR spectrum of **4** (Fig. 1). The ^{125}Te NMR spectrum of **1** showed a signal at δ 146.6 ppm (t, $^2J_{Te-H} = 25$ Hz), which compares with the ^{125}Te NMR signal for **2** at δ 336 (t, $^2J_{Te-H} = 24.9$ Hz) [11] and for $Fe_2(CO)_6(\mu\text{-}SCH_2Te)$ (**3**) at δ 39.1 ppm (t, $^2J_{Te-H} = 26$ Hz) (Fig. 2).

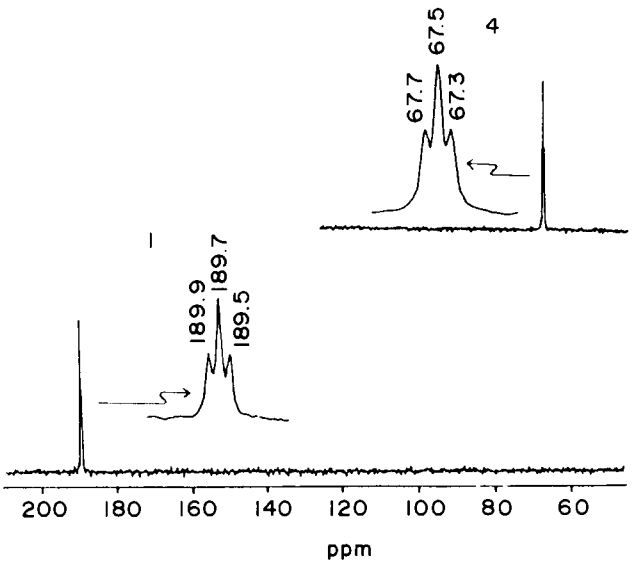

Fig. 1. ^{77}Se NMR spectra of $Fe_2(CO)_6(\mu\text{-}SeCH_2Te)$ (**1**) and $Fe_2(CO)_6(\mu\text{-}SeCH_2Se)$ (**4**).

2.2. Structure of $Fe_2(CO)_6(\mu\text{-}SeCH_2Te)$

Dark red hexagonal shaped crystals of **1** were obtained from a hexane/CH_2Cl_2 solvent mixture at −10°C and an X-ray diffraction study was undertaken. An ORTEP diagram of the molecular structure of **1** is shown in Fig. 3. The core geometry of **1** can be described as an open Fe_2SeTe butterfly tetrahedron in which the Se and Te atoms are located at the wing tips. The open edge of the Fe_2SeTe tetrahedron is bridged by a CH_2 group. Three terminally bonded carbonyl groups, the bridging Se or Te atoms and the Fe–Fe bond define the distorted octahedral geometry of each iron atom.

Overall, the structure of the methylene-substituted Fe_2SeTe core is similar to the structure of $Fe_2(CO)_6(\mu\text{-}TeCH_2Te)$ [5]. The average Fe–Se bond distance in **1** (2.454 Å) is somewhat longer than the average Fe–Se bond distances in $\{(CO)_6Fe_2(\mu\text{-}Se)_2\}_2C(Ph)\text{–}C(H)$ (2.368 Å), $Fe_2(CO)_6\{\mu\text{-}SeC(Ph)=C(H)Se\}$ (2.385 Å) [3], $\{(CO)_5Fe_2(\mu\text{-}Se)_2\}_2C(Ph)\text{–}C(H)(\mu\text{-dppe})$ (2.394 Å) [12] and $Fe_2(CO)_6Se_2Pt(PPh_3)_2$ (2.401 Å) [13]. However,

Table 1
Multinuclear NMR data (δ ppm) for compounds **1** and **3**

Compound	^1H NMR (δ w.r.t. TMS)	^{13}C NMR (δ w.r.t. TMS)	^{77}Se NMR (δ w.r.t. Me_2Se)	^{125}Te NMR (δ w.r.t. Me_2Te)
1	3.13 (s) $^2J_{H-Te} = 25$ Hz	−16.6 (t) $^1J_{C-H} = 159$ Hz 210.4 (s)	189.7 (t) $^2J_{Se-H} = 10$ Hz	146.6 (t) $^2J_{Te-H} = 25$ Hz
3	3.49 (s) $^2J_{H-Te} = 26$ Hz	5.8 (t) $^1J_{C-H} = 159$ Hz 209.8 (s)	– – –	39.1 (t) $^2J_{Te-H} = 26$ Hz

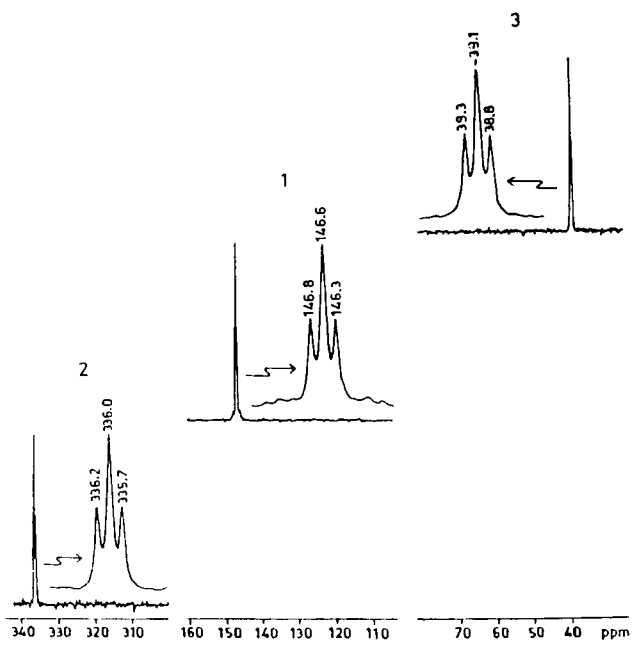

Fig. 2. ^{125}Te NMR spectra of $Fe_2(CO)_6(\mu$-$TeCH_2Te)$ (**2**), $Fe_2(CO)_6(\mu$-$SeCH_2Te)$ (**1**) and $Fe_2(CO)_6(\mu$-$SCH_2Te)$ (**3**).

the average Fe–Te bond distance in **1** (2.507 Å) is somewhat shorter than the average Fe–Te bond distances in **2** (2.546 Å), $[(\mu$-$CH_3Te)Fe_2(CO)_6]_2(\mu$-$TeCH_2Te$-$\mu)$ (2.553 Å) [6], $Fe_2(CO)_6[\mu$-$Te(CH_3)]_2$ (2.549 Å) [11] and $Fe_2(CO)_6\{\mu$-TeC(Ph)=C(H)Te} (2.523 Å) [14]. The Se(1)–C(7) bond length in **1** [2.021 (9) Å] is longer than the corresponding average Se–C bond lengths in $(CO)_6Fe_2Pt(PPh_3)_2\{\mu$-SeC(Ph)C(H)Se} (1.946 Å) [4] and $Fe_2(CO)_6\{\mu$-SeC(Ph)=C(H)Se} (1.94 Å), but similar to the average Se–C bond distances in $\{(CO)_6Fe_2(\mu$-$Se)_2\}_2C(Ph)$–C(H) (2.009 Å) and $\{(CO)_5$-$Fe_2(\mu$-$Se)_2\}_2C(Ph)$–C(H)(μ-dppe) (2.012 Å). The Te(1)–C(7) bond length in **1** [2.09(2) Å] is shorter than the average Te–C bond lengths in $Fe_2(CO)_6[\mu$-Te-$(CH_3)]_2$ (2.145 Å), $Fe_2(CO)_6[\mu$-$Te(CH_2)_2Te]$ (2.153 Å) [15], $[(\mu$-$CH_3Te)Fe_2(CO)_6]_2(\mu$-$TeCH_2Te$-$\mu)$ (2.155 Å) and **2** (2.163 Å).

The Fe(1)–Se–Fe(2) angle (62.7°) and the Fe(1)–Te–Fe(2) angle (61.2°) in **1** are, in general, similar to the corresponding angles in $Fe_2(CO)_6\{\mu$-SeC(Ph)=C-(H)Se} (63.6°), $Fe_2(CO)_6Se_2Pt(PPh_3)_2$ (63.7°), $\{(CO)_5$-$Fe_2(\mu$-$Se)_2\}_2C(Ph)$–C(H)(μ-dppe) (63.8°), $Fe_2(CO)_6(\mu$-$TeCH_2Te)$ (61.1°), $Fe_2(CO)_6\{\mu$-TeC(Ph)=C(H)Te} (61.3°), $Fe_2(CO)_6[\mu$-$Te(CH_3)]_2$ (62.3°) and $Fe_2(CO)_6$-$[\mu$-$Te(CH_2)_2Te]$ (62.6°), indicating a similar degree of opening of the Fe_2E_2 butterfly in all of these molecules. In contrast when larger species are inserted, such as in $\{Fe_2(CO)_6\}(\mu_4$-Te)(μ_3-Te){$Ru_3(CO)_{11}$}, the extent of opening of the Fe_2Te_2 butterfly unit is much greater (average Te–Fe–Te angle = 79°) [16]. The average Fe–Se–C(7) angle in **1** (89.5°) is smaller than the corresponding angles in $(CO)_6Fe_2Se_2\{\mu$-HC=C(C≡CCH_3)} (99.8°), $(CO)_6Fe_2Se_2(\mu$-HC=CC–$CCH_3)Os_3(CO)_{10}$ (100.5°), $\{(CO)_6Fe_2Se_2\}_2\{\mu$-HC–C(C≡$CCH_3$)} (102.9°) [17] and $\{(CO)_5Fe_2\{\mu$-$Se)_2\}_2C(Ph)$–C(H)(μ-dppe) (103.7°). The average Fe–Te–C(7) angle in **1** (86.5°) is smaller than the corresponding average angles in **2** (88.9°), $Fe_2(CO)_6[\mu$-$Te(CH_2)_3Te]$ (101.3°), $Fe_2(CO)_6$-$[\mu$-$Te(CH_3)_2]$ (109.1°) and $Fe_2(CO)_6[\mu$-$Te(CH_2)_3Te]$ (109.9°).

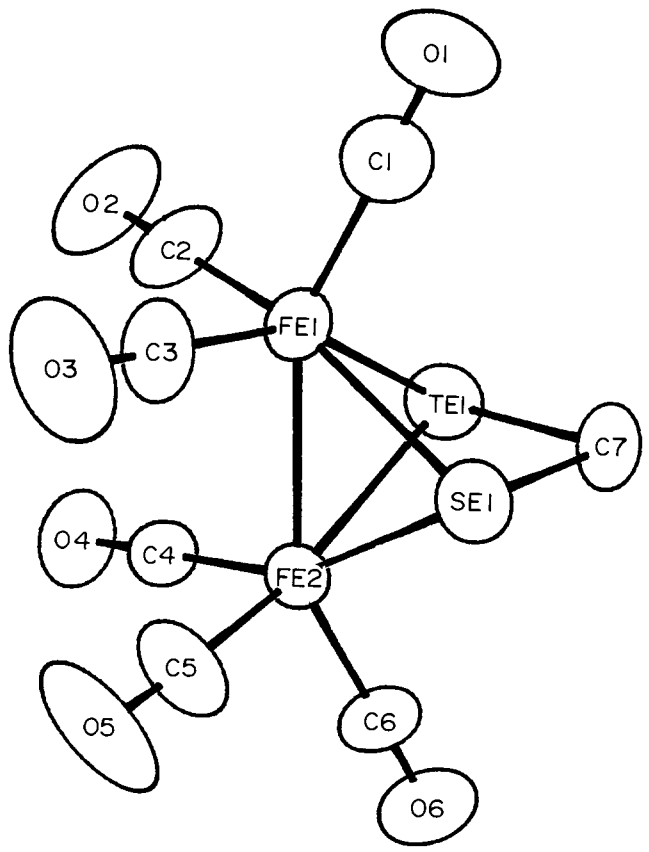

Fig. 3. ORTEP diagram of $Fe_2(CO)_6(\mu$-$SeCH_2Te)$ (**1**) (70% occupancy).

2.3. Reaction of $Fe_2(CO)_6(\mu$-STe) with diazomethane

The reaction of $Fe_2(CO)_6(\mu$-STe) with diazomethane was carried out following a similar procedure to that adopted for the reaction of $Fe_2(CO)_6(\mu$-SeTe) with diazomethane (Scheme 2). TLC indicated the formation of at least nine different compounds.

Of these, one was isolated in sufficient amount for a complete characterisation. It displayed an infrared spectrum in the carbonyl region which was similar to

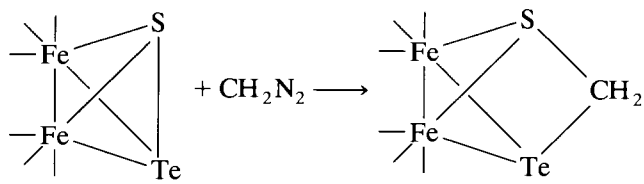

Scheme 2. Formation of compound **3**.

that of **2** with a shift of frequencies to higher values consistent with the replacement of Te by the less electropositive S atom. NMR spectroscopy (Table 1) and elemental analysis confirmed the identity of this compound as $Fe_2(CO)_6(\mu\text{-}SCH_2Te)$ (**3**). The ^1H NMR spectrum of **3** showed a single peak for the CH_2 protons at δ 3.49 ppm with ^{125}Te satellites ($^2J_{H-Te} = 26$ Hz). The ^1H-coupled ^{13}C NMR spectrum of **3** showed a triplet centred at δ 5.8 ppm ($^1J_{C-H} = 159$ Hz) for the CH_2 group and a single peak at δ 209.8 ppm due to the CO groups. The ^{125}Te NMR spectrum of **3** showed a signal at δ 39.1 ppm ($^2J_{Te-H} = 26$ Hz), as expected, upfield of the ^{125}Te NMR spectrum signal for **1** at δ 146.6 ppm ($^2J_{Te-H} = 25$ Hz) and for **2** at δ 336 ppm ($^2J_{Te-H} = 24.9$ Hz).

3. Experimental details

All the reactions were carried out under a pure and dry argon or nitrogen atmosphere with the use of standard Schlenk techniques. The solvents were purified, dried and distilled under a nitrogen or argon atmosphere prior to use, according to the literature methods. Infrared spectra were recorded on a Nicolet 5DXB FT spectrometer in sodium chloride cells of 0.1 mm path length as hexane solutions. ^1H, ^{13}C, ^{77}Se and ^{125}Te NMR spectra were obtained on a Varian VXR-3005 NMR spectrometer in $CDCl_3$ solution using appropriate references. The ^{77}Se NMR spectra were referenced to Me_2Se as an external standard ($\delta = 0$ ppm) and the spectra were obtained at an operating frequency of 57.23 MHz; 90° pulses were used with 1.0 s delay and 1.0 s aquisition time. ^{125}Te NMR spectra were referenced to Me_2Te as an external standard ($\delta = 0$ ppm) and the spectra were obtained at the operating frequency of 94.75 MHz; 90° pulses were used with 1.0 s delay and 1.0 s aquisition time. $Fe_2(CO)_6(\mu\text{-SeTe})$ and $Fe_2(CO)_6(\mu\text{-STe})$ were prepared as previously reported [7,8]. Diazomethane was prepared by dissolving 2.14 g of *N*-methyl-*N*-nitroso-*p*-toluenesulphonamide in 30 ml of diethyl ether and the solution cooled in ice. To this a solution consisting of 0.4 g of KOH in 10 ml of 96% ethanol was added. After 5 min the ethereal solution was distilled from a water bath. The ethereal solution contained 0.32–0.35 g of diazomethane [9].

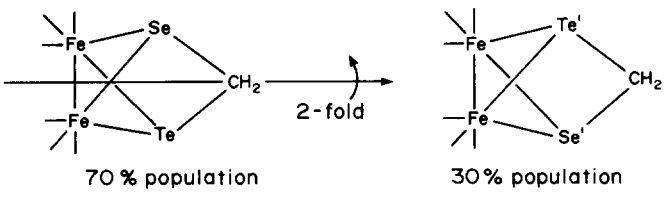

Fig. 4. Diagram showing the twofold axis disorder necessary to generate the molecule with the Te and Se sites exchanged (30% occupancy).

Table 2
Summary of crystallographic data for compound **1**

Crystal data	
Molecular formula	$C_7H_2O_6Se_1Te_1Fe_2$
Molecular weight	500.3
Space group	monoclinic, $P2_1/n$
Cell parameters	
a (Å)	6.695(2)
b (Å)	13.993(5)
c (Å)	14.007(4)
β (°)	103.03(2)
V (Å^3)	1278(7)
Z	4
No. of reflections and θ range (°) used for unit cell parameters	25, 12–14
Radiation used, λ (Å)	Mo Kα (0.7107)
D_{calc} (g cm^{-3})	2.599
Adsorption coeff., μ (cm^{-1})	73.4
Temperature (K)	295
Crystal colour and description	dark plates
Crystal dimensions (mm)	0.16×0.16×0.10
Data collection	
Diffractometer	Enraf-Nonius CAD-4
Scan mode	ω–2θ
Absorption correction	empirical
Transmission min., max.	66.5, 99.7
Measured reflections	3694
Observed reflections $I \geq 5\sigma(I)$	1850
θ_{max} (°)	30
h_{min}, h_{max}	0, 9
k_{min}, k_{max}	0, 19
l_{min}, l_{max}	−19, 19
No. of intensity control reflections, frequency and variation	3, every 1 h, nil
No. of orientation control reflections, frequency and variation	3, every 200 reflns., nil
Refinement	
Refinement on	$\|F\|$
Final R	0.030
Weighted R	0.047
Reflections used	1850
No. of parameters in the least-squares refinement	154
Hydrogen atom positions	not refined
(Δ/σ) max.	0.01
Weighting scheme, W	$1/\sigma^2(F)$
$\Delta\rho$ max. (e Å^{-3})	+0.49
$\Delta\rho$ min. (e Å^{-3})	−0.96
Extinction correction	applied
Source of atomic scattering factors	*International Tables for X-ray Crystallography*, 1974, Vol. IV

3.1. Reaction of $Fe_2(CO)_6(\mu\text{-SeTe})$ with diazomethane

To a solution of $Fe_2(CO)_6(\mu\text{-SeTe})$ (0.82 mmol) in dry diethyl ether (30 ml) was added dropwise an ethe-

real solution of diazomethane (24 mmol) (30-fold excess) by distilling a basic solution of *N*-methyl-*N*-nitroso-*p*-toluenesulphonamide in diethyl ether. Addition of diazomethane was continued until TLC and IR indicated total consumption of the $Fe_2(CO)_6(\mu$-SeTe) starting material. The reaction mixture was stirred at room temperature for a further 30 min. The solution was filtered through Celite and the solvent evaporated. The mixture was redissolved in petroleum ether and subjected to chromatographic work-up on silica gel TLC plates using petroleum ether as eluent. The orange coloured compound **1** {16 mg, 4% based on $Fe_2(CO)_6(\mu$-SeTe)} was obtained as the third band, m.p. 97–99°C. IR (ν, cm^{-1}): 2065 (m); 2026 (vs); 1995 (s); 1986 (s); 1975 (w). Anal. Found: C, 16.8; H, 0.37 $C_7H_2Fe_2O_6SeTe$ Calc.: C, 16.8; H, 0.39%.

3.2. Reaction of $Fe_2(CO)_6(\mu$-STe) with diazomethane

To a solution of $Fe_2(CO)_6(\mu$-STe) (0.82 mmol) in dry diethyl ether (30 ml) was added dropwise an ethereal solution of diazomethane (24 mmol) (30-fold excess) by distilling a basic solution of *N*-methyl-*N*-nitroso-*p*-toluenesulphonamide in diethyl ether. Addition of diazomethane was continued until TLC and IR indicated total consumption of $Fe_2(CO)_6(\mu$-STe) starting material. The reaction mixture was stirred at room temperature for further 30 min. The solution was filtered through Celite and the solvent evaporated. The mixture was redissolved in petroleum ether and subjected to chromatographic work-up on silica gel TLC plates using petroleum ether as eluent. The orange coloured compound **3** {11 mg, 3% based on $Fe_2(CO)_6(\mu$-STe)} was obtained as the fifth band, m.p. 73–75°C. IR (ν, cm^{-1}): 2068 (m); 2029 (vs); 1999 (s); 1989 (s); 1976 (sh). Anal. Found: C, 18.3; H, 0.54. $C_7H_2Fe_2O_6STe$ Calc. C, 18.5; H, 0.44%.

3.3. X-Ray diffraction study of compound 1

Single crystal X-ray data were collected on an Enraf-Nonius CAD-4 diffractometer. The structure was solved via the heavy-atom method by locating the position of the heaviest atom Te in the Patterson map. The remaining atoms appeared in the subsequent difference Fourier maps alternated with the least-squares refinement of the input atoms. The two hydrogen atoms, stereochemically fixed, were not refined. The full-matrix least-squares refinement of all the atoms converged to an *R* index of 0.060 ($Rw = 0.066$), but the final difference map contained a positive electron density of 4.3 e $Å^{-3}$ at the site of Se(1) and a negative electron density of 3.0 e $Å^{-3}$ at the site of Te(1). These features remained constant after applying the extinction correction and raising the criterion of observed reflections from 3σ to 5σ (an empirical absorption

Table 3
Final positional parameters of non-H atoms with their isotropic equivalent β-factors

Atom	*x*	*y*	*z*	$B(Å^2)$ [a]
Te(1)	0.2283(1)	0.19330(6)	0.17009(7)	4.63(1)
Te(1′)	0.672	0.133	0.211	3.8*
Se(1)	0.6720(1)	0.13330(8)	0.21133(8)	3.89(2)
Se(1′)	0.228	0.193	0.170	2.1*
Fe(1)	0.4750(2)	0.17565(8)	0.33329(7)	3.65(2)
Fe(2)	0.3773(1)	0.03211(6)	0.21983(7)	3.22(1)
O(1)	0.164(2)	0.1372(6)	0.8859(8)	7.6(2)
O(2)	0.136(2)	0.187(1)	0.4334(6)	9.3(3)
O(3)	0.732(3)	0.0637(9)	0.4887(9)	10.7(3)
O(4)	0.0370(9)	0.9697(6)	0.3031(5)	5.6(1)
O(5)	0.369(1)	0.1191(5)	0.673(1)	8.9(2)
O(6)	0.728(2)	0.0595(8)	0.9735(7)	8.5(2)
C(1)	0.086(2)	0.2075(7)	0.8636(8)	5.4(2)
C(2)	0.270(2)	0.181(1)	0.3962(7)	6.2(2)
C(3)	0.631(2)	0.1071(8)	0.4290(7)	5.9(2)
C(4)	0.834(1)	0.0053(5)	0.7317(5)	3.7(1)
C(5)	0.462(1)	0.0601(6)	0.7158(9)	5.4(2)
C(6)	0.688(1)	0.0225(7)	0.8991(6)	4.9(2)
C(7)	0.487(2)	0.2185(7)	0.1131(6)	4.9(2)

[a] Starred atoms were refined isotropically. Anisotropically refined atoms are given in the form of the isotropic equivalent displacement parameter defined as: $\frac{4}{3}[a^2B_{1,1} + b^2B_{2,2} + c^2B_{3,3} + ab(\cos\gamma)B_{1,2} + ac(\cos\beta)B_{1,3} + bc(\cos\alpha)B_{2,3}]$.

Table 4
List of selected bond lengths (Å) [a]

Te(1)–Fe(1)	2.512(1)	Fe(2)–C(4)	1.783(8)
Te(1)–Fe(2)	2.502(1)	Fe(2)–C(5)	1.788(8)
Te(1)–C(7)	2.09(2)	Fe(2)–C(6)	1.795(9)
Se(1)–Fe(1)	2.455(2)	O(1)–C(1)	1.12(1)
Se(1)–Fe(2)	2.453(1)	O(2)–C(2)	1.13(2)
Se(1)–C(7)	2.021(9)	O(3)–C(3)	1.13(2)
Fe(1)–C(1)	1.81(2)	O(4)–C(4)	1.14(2)
Fe(1)–C(2)	1.79(1)	O(5)–C(5)	1.12(1)
Fe(1)–C(3)	1.78(2)	O(6)–C(6)	1.14(1)

[a] Numbers in parentheses are estimated standard deviations in the least significant digits.

Table 5
List of selected bond angles (°) [a]

Fe(1)–Te(1)–Fe(2)	61.24(4)	Te(1)–Fe(2)–C(5)	161.5(3)
Fe(1)–Te(1)–C(7)	86.2(2)	Te(1)–Fe(2)–C(6)	97.3(3)
Fe(2)–Te(1)–C(7)	86.9(3)	C(4)–Fe(2)–C(5)	92.0(4)
Fe(1)–Se(1)–C(7)	89.3(3)	C(4)–Fe(2)–C(6)	100.5(4)
Fe(2)–Se(1)–C(7)	89.8(3)	C(5)–Fe(2)–C(6)	98.8(5)
Te(1)–Fe(1)–C(1)	106.0(3)	Fe(1)–C(1)–O(1)	176(1)
Te(1)–Fe(1)–C(2)	91.4(3)	Fe(1)–C(2)–O(2)	178(1)
Te(1)–Fe(1)–C(3)	153.0(4)	Fe(1)–C(3)–O(3)	179(1)
C(1)–Fe(1)–C(2)	99.6(6)	Fe(2)–C(4)–O(4)	176.9(6)
C(1)–Fe(1)–C(3)	99.9(5)	Fe(2)–C(5)–O(5)	176(2)
C(2)–Fe(1)–C(3)	92.2(6)	Fe(2)–C(6)–O(6)	178(1)
Te(1)–Fe(2)–C(4)	94.1(2)		

[a] Numbers in parentheses are estimated standard deviations in the least significant digits.

correction was already applied to the intensity data).

This behaviour was interpreted as a statistical twofold disorder about the axis passing through the midpoint of Fe(1) and Fe(2) and C(7), bringing one-half of the molecule into coincidence with the other half, except that the Te and Se sites became admixed (Fig. 4). The occupancies were assigned as 70% and 30% so as to fit the residual electron densities observed in the final difference map. The positional parameters of the minor sites Te(1′) and Se(1′) were kept fixed and only the isotropic temperature factors were allowed to refine until convergence was reached. Invoking this disordered model brought the R-value down dramatically to 0.030 ($Rw = 0.047$), and the final difference Fourier was clear with no significant $\Delta\rho$, either positive or negative, near the Te and Se sites. Crystallographic data for **1** are summarised in Table 2. Final positional parameters of the non-hydrogen atoms with their isotropic equivalent B-factors and lists of selected bond lengths (Å) and angles (°) are given in Tables 3–5. General displacement parameters, bond distances and angles and the structure factor tables are available from the authors.

Acknowledgement

The Department of Atomic Energy, Government of India is thanked for financial support (to P.M.).

References

[1] K.H. Whitmire, *J. Coord. Chem., 17* (1988) 95; N.A. Compton, R.J. Errington and N.C. Norman, *Adv. Organomet. Chem., 31* (1990) 91; L.C. Roof and J.W. Kolis, *Chem. Rev., 93* (1993) 1037.
[2] P. Mathur, D. Chakrabarty and I.J. Mavunkal, *J. Cluster Sci., 4* (1993) 351.
[3] P. Mathur and Md.M. Hossain, *Organometallics 12* (1993) 2398.
[4] P. Mathur, Md.M. Hossain, K. Das and U.C. Sinha, *J. Chem. Soc., Chem. Commun.*, (1993) 46.
[5] P. Mathur, V.D. Reddy and R. Bohra, *J. Organomet. Chem., 401* (1991) 339.
[6] P. Mathur, V.D. Reddy, K. Das and U.C. Sinha, *J. Organomet. Chem., 409* (1991) 255.
[7] P. Mathur, D. Chakrabarty and Md.M. Hossain, *J. Organomet. Chem., 401* (1991) 167.
[8] P. Mathur, D. Chakrabarty, Md.M. Hossain and R.S. Rashid, *J. Organomet. Chem., 420* (1991) 79.
[9] A.I. Vogel, *Textbook of Practical Organic Chemistry*, 4th edn., ELBS, Longman, 1984, p. 291.
[10] P. Mathur, B. Manimaran, Md.M. Hossain and M. Arabatti, unpublished results.
[11] R.E. Bachman and K.H. Whitmire, *Organometallics, 12* (1993) 1988.
[12] P. Mathur, Md.M. Hossain and M.F. Mahon, *J. Organomet. Chem., 471* (1994) 185.
[13] V.W. Day, D.A. Lesch and T.B. Rauchfuss, *J. Am. Chem. Soc., 104* (1982) 1290.
[14] T. Fassler, D. Buchholz, G. Huttner and L. Zsolnai, *J. Organomet. Chem., 369* (1989) 297.
[15] M. Shieh and M.-H. Shieh, *Organometallics, 13* (1994) 920.
[16] P. Mathur, I.J. Mavunkal and A.L. Rheingold, *J. Chem. Soc., Chem. Commun.*, (1989) 382.
[17] P. Mathur, Md.M. Hossain and A.L. Rheingold, unpublished results.